

# Reducing Cost but not Quality with Digital Scanner Interfaces for Optical Coherence Tomography

Kyoungmo Koo,<sup>1</sup> Lucia Lee,<sup>1</sup> Morgan McCloud,<sup>3</sup> and Mark Draelos<sup>1,2</sup>

<sup>1</sup>*Department of Robotics, University of Michigan*

<sup>2</sup>*Department of Ophthalmology and Visual Sciences, University of Michigan Medical School  
2505 Hayward St, Ann Arbor, MI 48109, USA*

[mdraelos@umich.edu](mailto:mdraelos@umich.edu)

<sup>3</sup>*Department of Biomedical Engineering, Duke University  
100 Science Dr, Durham, NC 27708, USA*

## ABSTRACT (100)

Optical coherence tomography (OCT) systems are traditionally decomposed into engine and scanner components with an expensive and noise-prone analog interface to communicate the scan pattern between the two. To overcome these limitations, we implement a digital interface for our OCT system using low-cost embedded microprocessor and custom PC software. We demonstrate quantitative and qualitative equivalence of the interfaces to the theoretical optical resolution limits of our scanner through signal and image quality metrics, despite an order of magnitude reduction in cost. These results demonstrate the potential for reducing costs without sacrificing image quality through digital interfacing.

## ABSTRACT (250)

Optical coherence tomography (OCT) systems are traditionally decomposed into engine and scanner components with an expensive and noise-prone analog interface to communicate the scan pattern between the two. Although simple and convenient, analog signals are susceptible to interference and require expensive hardware to generate with appropriate precision for OCT. To overcome these limitations, we implemented a digital interface for our OCT system using low-cost embedded microprocessor and custom PC software, exploiting recent trends towards digital servo drivers for optical scanning. Our interface features USB interfacing with a PC for scan pattern download and position feedback upload, 50 kHz communication rate, external triggers with adjustable downsampling, and no external power requirements. We characterize the latency and noise of this digital interface and the quality of the resulting OCT images in direct comparison to a traditional analog interface that costs ten times more. Signal analysis reveals that the digital interface accurately communicated the scan pattern to the galvanometer driver and considerably reduced noise in the position feedback signal. Resolution tests show that the digital interface performs as well as the standard analog interface to the resolution limits of our OCT scanner. Together, these results demonstrate quantitative and qualitative equivalence of the interfaces, despite an order of magnitude reduction in cost. We plan to release open-source software, schematics, design files, and a bill of materials so that the OCT research community can benefit from these improvements and cost savings.

**Keywords:** optical coherence tomography, digital control, galvanometers, embedded systems

# Reducing Cost but not Quality with Digital Scanner Interfaces for Optical Coherence Tomography

Kyoungmo Koo,<sup>1</sup> Lucia Lee,<sup>1</sup> Morgan McCloud,<sup>3</sup> and Mark Draelos<sup>1,2</sup>

<sup>1</sup>Department of Robotics, University of Michigan

<sup>2</sup>Department of Ophthalmology and Visual Sciences, University of Michigan Medical School  
2505 Hayward St, Ann Arbor, MI 48109, USA

[mdraelos@umich.edu](mailto:mdraelos@umich.edu)

<sup>3</sup>Department of Biomedical Engineering, Duke University

100 Science Dr, Durham, NC 27708, USA

## 1. INTRODUCTION

Optical coherence tomography (OCT) systems traditionally consist of two system-level components: the engine, which forms the interferometric signal from reference and sample arm light, and the scanner, which controls the spatial distribution of sample arm light. High-quality OCT imaging requires precise synchronization between the engine and scanner so that the captured data is reconstructed at the correct spatial position. The choice of scanner technology and interface between the engine and scanner is therefore a major consideration in OCT system design, and system designers go to great lengths to optimize scanner performance [1]. A common selection, especially in research and academic settings, is an analog interface in which the engine encodes the target scan position as a voltage that the scanner then senses.

Although simple and convenient, the analog interface is problematic for two reasons. First, analog signals are susceptible to interference and degradation from electromagnetic noise, temperature fluctuations, attenuation over long distances, and variations in reference point. The command that the scanner senses may consequently differ from what the engine expected. Second, the precise nature of OCT demands high-quality analog interface hardware with 16-bit resolution and low-noise characteristics. Hardware for this purpose from typical vendors (e.g., National Instruments) costs several thousand US dollars yet is still susceptible to the aforementioned issues. We believe that the OCT community would benefit from an alternative engine-scanner interface that exhibits reduced noise and low latency, has 16-bit or better resolution, provides bidirectional communication (position commands and feedback), is created from low-cost components, and is robust and easy to use.

To meet these requirements, we implemented a digital interface for our OCT system using low-cost components from STMicroelectronics' established STM32 ecosystem of embedded microprocessors (Fig. 1), exploiting trends towards digital servo drivers for optical scanning [2,3]. Our reference OCT scanner is based on the Mach-DSP servo driver (Pangolin Laser Systems; Sanford, FL), which supports both analog and digital communication modes. In this summary, we describe the design and implementation of our digital interface with parts totaling less than \$100 USD. Our interface features USB interfacing with a PC for scan pattern download and position feedback upload, 50 kHz communication rate, external triggers with adjustable downsampling, and no external power requirements. We characterize the latency and noise of this digital interface and the quality of the resulting OCT images in direct comparison to a traditional analog interface that costs ten times more. We plan to release open-source software, schematics, design files, and a bill of materials so that the OCT research community can benefit from these improvements and cost savings.

### 2.1 System architecture

For implementation of our digital interface, we designed a swept-source OCT engine with a scanner based on Saturn 1B galvanometers (ScannerMAX; Sanford, FL) and a Mach-DSP servo driver. This driver implements the vendor-specific FB4 digital communication protocol for exchange of 16-bit position commands and feedback over a 4-wire 3.3 V TTL connection in real-time at up to a few hundred kHz. This allows users to send position data to and receive feedback from the galvanometer driver without analog signal noise or expensive digital-analog conversion hardware. Unfortunately, a PC is not able to implement custom board-level protocols nor reach these control rates with a typical multi-tasking operating system. Thus, the primary goal of our digital interface is to provide a bridge for our control PC over a USB connection so that it can communicate in real-time with the MachDSP over FB4. Constructing a digital interface suitable for scanning thus involves integrating three critical functions. First, we must communicate in real-time with the Mach-DSP over the FB4 protocol. Second, we must communicate with the control PC over USB and buffer the position commands/feedback for it. Third, we must output the buffer scan pattern to the Mach-DSP in synchronization with the laser trigger. To deliver these multiple functions, we employed the Nucleo-64 L476RG evaluation board from STMicroelectronics, which we subsequently refer to as the "STM32." The STM32 features an ARM Cortex-M4 CPU as well as an extensive range of peripherals and communication protocols. Furthermore, its cost-effectiveness, compact size, and mature development ecosystem make it highly practical and broadly applicable.

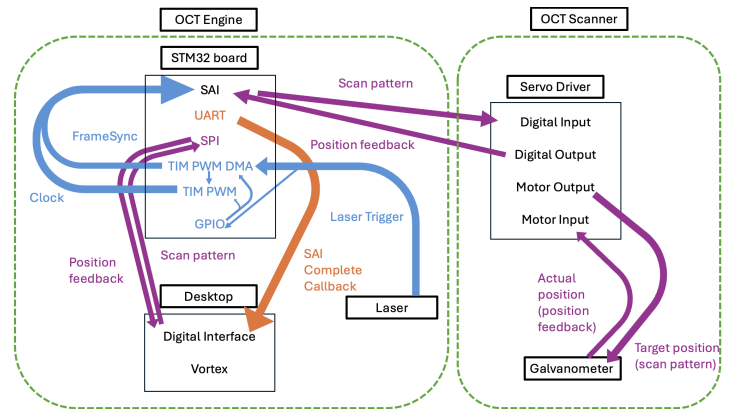


**Figure 1.** Overview of the digital scanner interface. Once a laser trigger signal activates the timer interface, the SAI bus begins data exchange between the STM32 board and the servo driver. Each callback function of the SAI transmission subsequently triggers UART and SPI communication (TX/RX) between the desktop and the STM32 board. This entire process is synchronized with the laser trigger signal, enabling continuous generation of OCT scan waveforms.

## 2. APPROACH

## 2.2 Data exchange with Mach-DSP and PC

The FB4 protocol is vendor-specific and different from standard board-level protocols like SPI or I<sup>2</sup>C; however, we can leverage the STM32's serial audio interface (SAI) peripheral to implement FB4 with a specialized configuration (Fig. 1, purple). Specifically, we configure the SAI interface with clock strobing set to low, a frame synchronization pulse width of 1 bit, and the data size, slot size, and frame length all set to 32 bits. For buffering, we divide transmit (TX) and receive (RX) buffers within the the SAI interface into two halves, synchronized such that as TX completes transmitting data in one half, RX concurrently finishes receiving data in the corresponding half. To avoid conflicts, the computer must operate on the buffer half not currently accessed by SAI. For instance, while SAI is processing the first half, the PC can safely write and read data in/from the second half of the buffers. Upon completion of half the SAI transmission and reception, a callback function notifies the desktop to initiate data handling for the first half of the buffer, with a similar process for the second half. The STM32 board uses UART over USB to communicate with the desktop, sending a message each time the SAI callback functions are triggered (Fig. 1, orange). Following the reception of a UART message, the STM32's SPI peripheral was utilized for transmission of recent position feedback it received, and reception of new scan pattern from computer. Direct memory access and callback functions were employed to integrate peripherals in the correct sequence without interrupting each other.

## 2.3 Synchronization with laser trigger

The scan position data must be synchronized with the start of OCT acquisition and each laser sweep in order to produce an accurate image. Moreover, the scan pattern sampling rate may be different from the laser sweep rate due to hardware restrictions. We provide these features through the STM32's IO and timer peripherals (Fig. 1, blue). Once armed by the PC for the start of acquisition, the STM32 waits for laser trigger pulse. When the pulse arrives, the timer interface generates the bit clock and frame synchronization signals for FB4 through a combination of downsampling and upsampling of the laser trigger. These signals are wired externally into the SAI module to provide an external bit clock at the desired frequency. We use the timer's waveform generation capabilities channel to produce a continuous clock and frame synchronization signal with the necessary pulse widths.

## 2.4 Timing diagram for full system

Figure 2 illustrates the timing diagram of the overall system. The continuous exchange of scan patterns and position feedback between the STM32 and the servo driver occurs via the SAI/FB4 protocol. When the callback function is triggered after each half of the buffer is transmitted and received, the STM32 notifies the desktop via UART. Subsequently, the desktop, acting as the leader, begins sending the clock signal, and the STM32 sends the recently received position feedback from the servo driver back to the desktop. After receiving the position feedback, the desktop transmits data via the SPI bus into the half of the scan pattern buffer in the STM32 that was just sent. A crucial assumption of this timing diagram is that the time spent on TX/RX for half of the buffer in the SAI part must be longer than the preparation time. The preparation time includes notification via UART and the transmission and reception of each chunk via the SPI bus. We determined the maximum possible communication rate to be 62.5 kHz, limited by this particular STM32's UART and SPI bitrates.

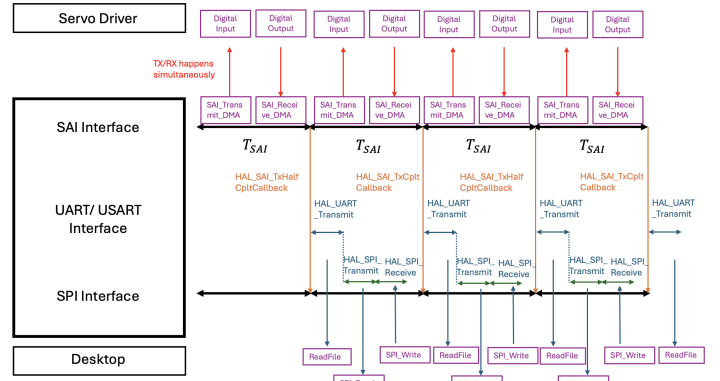


**Figure 2.** Timing diagram of the system. Continuous exchange of scan patterns and position feedback occurs between the STM32 and the servo driver via the SAI/FB4 protocol. The diagram includes the notification process via UART, the leader clock signal from the desktop, and data transmission via SPI.

The STM32 board uses UART over USB to communicate with the desktop, sending a message each time the SAI callback functions are triggered (Fig. 1, orange). Following the reception of a UART message, the STM32's SPI peripheral was utilized for transmission of recent position feedback it received, and reception of new scan pattern from computer. Direct memory access and callback functions were employed to integrate peripherals in the correct sequence without interrupting each other.

## 3. METHODS

We evaluated our digital interface for OCT imaging with regards to its reduction of noise in the position feedback signals and its effect on image quality as compared to PCIe-6363 analog interface (National Instruments; Austin, TX).

### 3.1 Characterization of signal noise

Inevitable discrepancies arise between the commanded and sensed positions of the galvanometer, including interface errors (e.g., noise), fixed response delays, and galvanometer tracking errors. The magnitude of these errors not only elucidates the performance degradation of the generated image but also serves as a metric for evaluating the superiority of different systems. We therefore performed imaging with the same scan waveform separately using the analog and digital interfaces. In order to isolate the effect of interface errors, we corrected for fixed response delays and used identical galvanometer tunings. We then compared the position feedback to the ideal commanded position from the PC and computed the tracking error. We quantified noise using the standard deviation of the error signal.

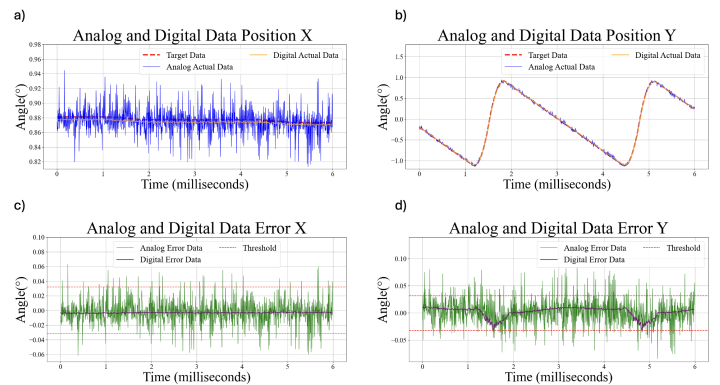


**Figure 3.** Path tracking performance (blue/orange) and errors (green/purple) for analog and digital interfaces. The analog interface exhibits more than twice the noise amplitude of the digital interface. Dashed horizontal red line denotes theoretical resolution limit of our scanner converted to galvanometer angle.

### 3.2 Characterization of image quality

Beyond noise characteristics, the digital interface must also produce equivalent or better image quality than the analog interface. The USAF-1951 resolution target was employed to compare the resolution limits between images generated via analog and digital interfaces. We acquired OCT data over an approximately  $0.8 \times 0.8$  mm field of view at  $512 \times 512$  px to capture groups 4 and 5. We obtained 5 volumes each with the analog and digital interfaces without moving the target. We averaged these volumes together, generated a maximum intensity projection, and extracted profiles across the elements.

### 3.3 OCT system

For both experiments, we used our lab standard OCT system built with a 200 kHz 1060 nm swept source laser (Thorlabs; Newton, NJ) which illuminated a Mach-Zehnder interferometer. A 1 GHz balanced receiver (Thorlabs; Newton, NJ) was used to measure the interferometric signal, which was subsequently detected using a  $1.0 \text{ GS s}^{-1}$  digitizer (ATS-9364, Alazar Technologies, Inc.; Pointe-Claire, Quebec). OCT signal generation and processing were performed with custom GPU-accelerated software written in Python using *vortex* [4]. We acquired images using a telecentric scanner with 47.7 mm working distance, Airy radius of  $29 \mu\text{m}$  over a 32 mm field of view, and ScannerMax galvanometers operating with hand-tuned PID control parameters.

## 4. RESULTS & DISCUSSION

### 4.1 Signal noise

We determined the response delay by comparing the actual and target positions and selecting the delay that produced the minimum root mean square error (RMSE). For the analog interface, the optimal delay was 18 samples ( $90 \mu\text{s}$ ), while for the digital interface, it was 5 samples ( $100 \mu\text{s}$ ). Errors attributed solely to the interface, after excluding those caused by time delay, had the following RMSE and standard deviation (Fig. 3). With the analog interface, we calculated  $0.0188 \pm 0.0185^\circ$  for the  $x$  axis and  $0.0239 \pm 0.0241^\circ$  for the  $y$  axis. With the digital interface, these values were  $0.0098 \pm 0.0074$  for the  $x$  axis and  $0.0095 \pm 0.0092$  for the  $y$  axis. The standard deviations for analog interface were approximately  $2.5\times$  larger than for the digital interface. These results first demonstrate that our digital interface accurately communicated the scan pattern to the galvanometer driver and second show that the digital interface considerably reduces noise in the position feedback signal. Notably, the digital interface produced errors below our theoretical lateral resolution (when converted to scan angle) whereas the analog interface exhibited frequent excursions beyond it.

### 4.2 Image quality

Both interfaces successfully resolved all elements of group 4, for both horizontal and vertical line pairs, as can be seen in Fig. 4. Consequently, our focus shifted to detailed analysis of the elements in group 5. The elements that showed the resolution limits for analog or digital interface were elements 2–4 for horizontal line pairs and elements 3–5 for vertical line pairs. For horizontal line pairs, element 2 exhibited clear contrast for both the analog and digital interfaces. However, this contrast diminished progressively for element 3 and ultimately failed to produce meaningful contrast for element 4. A similar phenomenon was observed on the vertical side, starting with a resolvable element 3 and progressing to unresolvable element 5.

Overall, line plots of these elements suggest that both interfaces exhibited similar performance for imaging applications. Although the digital interface demonstrated superiority over the analog interface in terms of target tracking error, both interfaces exhibited comparable performance in resolution. Thus, the digital interface performs as well as the standard analog interface to the resolution limits of our OCT scanner. The presence of increased noise in the analog position feedback waveforms suggests that we may be able to detect a difference using a scanner with higher theoretical resolution.

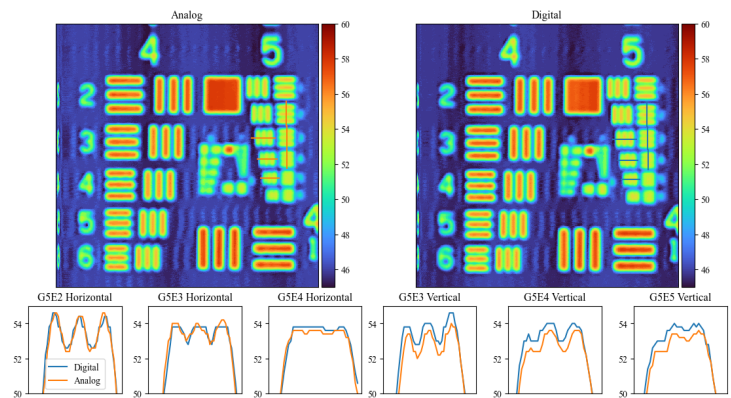


**Figure 4.** Comparison of analog (orange) and digital (blue) interfaces scanning groups 4 and 5 of a USAF target and plots through specific elements. Both interfaces resolve down to group 5 element 3 or element 4 for horizontal and vertical line pairs, respectively, demonstrating equivalent performance to the resolution of our scanner. Note scanner flyback artifact on left edge since we disabled *vortex*'s galvanometer latency correction for these experiments.

## 5. CONCLUSION

We demonstrate equivalent or better performance of our digital interface as compared to a typical analog interface with regards to signal integrity (e.g., noise) and resulting image quality. For future experiments, we plan to build a scanner with higher optical resolution since analog signal noise is of insufficient amplitude to affect our results. Additionally, we plan to release software, schematics, and a bill of materials so that others can replicate this digital interface, as well as incorporate support for it in our open-source OCT library *vortex*.

## REFERENCES

1. E. M. Tang and Y. K. Tao, "Modeling and optimization of galvanometric point-scanning temporal dynamics," *Biomed. Opt. Express*, vol. 12, no. 11, pp. 6701–6716, Nov 2021.
2. G. Chen and Y. Wang, "Control of a digital galvanometer scanner using a discrete-time sliding-mode variable-structure controller based on a decoupled disturbance compensator," *Applied Sciences*, vol. 11, no. 21, 2021.
3. Z. Xuan *et al.*, "Design of high-speed and high-precision scanning galvanometer control system based on FPGA+DSP architecture," in *2021 IEEE Sustainable Power and Energy Conference (iSPEC)*, 2021, pp. 3455–3459.
4. M. Draelos, "Vortex – an open-source library for building real-time OCT engines in C++ or Python," 2022.